Is Indirect Electrode a Good Choice for Simulated Lightning Damage Tests?—The Effect of Metal Vapor

Yakun Liu, *Member, IEEE*, and Yeqing Wang

***Abstract*— The laboratory lightning testing commonly uses an indirect electrode as the current injection configuration to restraint the electrode jet for evaluation of lightning strike damage tolerance of aircraft materials. Such an indirect electrode configuration requires using a conductive ignition wire to initiate the arc. This work discusses the influence of added metal vapor, produced due to evaporation of the ignition wire, on the electric-arc-induced heat flux and current density as well as the material damage through numerical modeling and simulated experiments. Metal vapor originated from the requisite ignition wire considerably alters the net emission coefficient and transport properties of the arc, leading to questionable testing results and unreliable guidance for lightning protection design. The damage depth of an aluminum alloy is affected by 312.5% due to the changes in the net emission coefficient and thermal conductivity. The damage area shows moderate changes due to a Gaussian-shape decrease profile of heat flux and its insensitivity to the changes in the net emission coefficient. The direct electrode configuration is promising to avoid the use of ignition wire and produce material damage representative of actual damage caused by natural lightning. The results and discussions provide insights into the design of improved lightning certification tests.**

***Index Terms*— Damage, direct electrode testing, indirect electrode, lightning, metal vapor.**

I. Introduction

LIGHTNING hazard is a serious concern to a wide range of objects, systems, and even to human activities, particularly drawing special attention to aircraft, wind turbines, electric transmission lines, oil tanks, and bridge cables, and so on [1]–[4]. There are ∼8 million lightning flashes occurring worldwide every day in stormy-weather regions covering over ∼10% of the earth's surface [5]. Meanwhile, global lightning manifests an increasing trend with the global temperature rise and added aerosol due to anthropogenic pollution [6]. In-flight statistics show that every commercial airliner is struck by lightning about once every 3000 h of flight time [7]. Moreover, ∼60% of fires in oil tanks are attributed to lightning [8]. Therefore, lightning protection is of great importance for industrial and human activities.

The direct damage effect is one of the deleterious effects of lightning, for which the overloads of the intense current and voltage injection, strong electromagnetic forces, high-pressure wave impacts, and massive heat infliction are the damage sources for lightning-attached materials [9]–[14]. For materials (e.g., metallic materials and fiber-reinforced polymer matrix composite materials), the damage responses, such as the damage area, depth, delamination, and residual strength, are key parameters in lightning testing [15], [16]. Limited by the uncertainty in natural lightning, the simulated lightning technology is a feasible method for lightning certification tests on materials. In the laboratory, the existing lightning simulation method mainly satisfies the current parameters for material testing but is compromised in the output voltage by reducing the discharge distance to several centimeters, as the extremely high power in lightning discharge (a peak voltage of $\sim 10^8$ V driving a peak current of hundreds of kA) overshoots the power rating of typical capacitors.

The lightning testing results are affected by the experimental setup. First, the electrodes with different geometries used in laboratory can result in different levels of damage results. For example, an aluminum plate with a thickness of 3.5 mm experienced burn-through when using an electrode with a semiellipsoidal or conical shape, but survived in the use of a hemispherical electrode with a damage depth of only 3 mm. The difference can reach as large as 2 times in damage depth and 2.4 times in damage area by adopting electrodes in different configurations (e.g., shapes and sizes) [17]. Furthermore, it has been reported that the size of the electrode has a significant impact on the degree of failure for carbon-fiber-reinforced polymer matrix composites [18]. The delamination area caused by an electrode with a diameter of 16 mm is almost 3 times larger than that caused by an electrode with a diameter of 98 mm [18]. The indirect electrode configuration (see Fig. 1), with an insulation cap on head, has been recommended to suppress the electrode jet in the lightning testing standards at present [19]–[23]. However, the indirect electrode setup requires using a conductive ignition wire to initiate the arc

Manuscript received December 28, 2020; accepted April 7, 2021. This work was supported in part by the National Key Research and Development Program of China under Grant 2017YFC1501506 and in part by the National Natural Science Foundation of China under Grant 51977129. The review of this article was arranged by Senior Editor K. W. Struve. *(Corresponding author: Yakun Liu.)*

Yakun Liu is with the Department of Electrical Engineering, Shanghai Jiao Tong University, Shanghai 200030, China, and also with the Massachusetts Institute of Technology, Cambridge, MA 02139 USA (e-mail: liuyakunhv@163.com).

Yeqing Wang is with the Department of Mechanical and Aerospace Engineering, Syracuse University, Syracuse, NY 13244 USA (e-mail: ywang261@syr.edu).

Color versions of one or more figures in this article are available at https://doi.org/10.1109/TPS.2021.3073534.

Digital Object Identifier 10.1109/TPS.2021.3073534

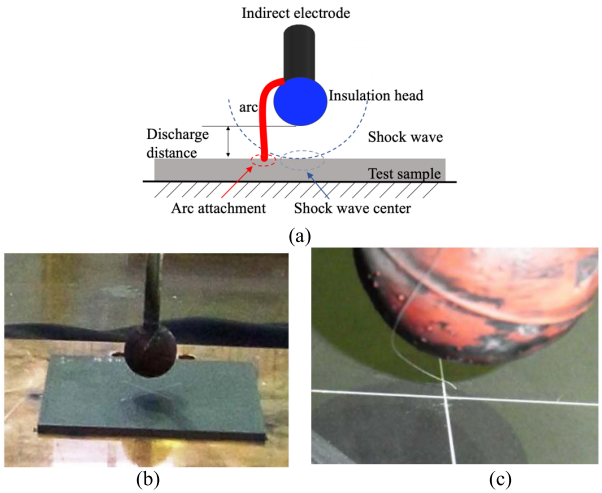

Fig. 1. (a) Schematic of the indirect electrode configuration, (b) photograph of the indirect electrode, and (c) initiation wire setup used to initiate the arc when using the indirect electrode configuration [19].

[see Fig. 1(c)], which will contaminate the discharge arc caused by the metal vapor due to material evaporation, and thus, considerably changing the properties of arc plasma. This problem has not been fully addressed in current lightning research to the authors' knowledge. The content of the metal vapor contamination is also different from one experiment to another, leaving the cross-comparison obscure between different research works.

Moreover, it is still unfeasible in the laboratory to directly measure the net emission coefficient and transport properties within the arc channel in a way with acceptable accuracy and resolution during lightning arc discharges. Meanwhile, the damage response of materials to the changes in net emission coefficient and transport properties needs to be considered by accounting for the coupling between lightning arc and materials. Therefore, in this work, the effects of metal vapor on the simulated lightning strike tests are studied by a numerical unified plasma material finite-element model (UPM-FEM). Since the metal vapor results in changes in the transport properties and the net emission coefficient of the plasma, the effect of the added metal vapor is investigated through an extensive parametric study aiming to determine the electric arc characteristics (e.g., heat flux, current density) and the corresponding material damage at varying plasma transport properties and net emission coefficients. The numerical implementation of the UPM-FEM is introduced in Section II. Analyses on the effect of metal vapor on the heat flux and current density as well material damage are detailed in Section III. Discussions on the indirect and direct electrodes are presented in Section IV. Conclusions are stated in Section V.

II. Numerical Implementation of UPM-FEM

The UPM-FEM models the arc–material interactions in a domain of the cathode–plasma–anode based on the magnetohydrodynamics (MHD) method [24]. The arc plasma is assumed to be in a local thermodynamic equilibrium (LTE) condition in the core region and regarded as a continuous domain of an electrically and thermally conductive fluid.

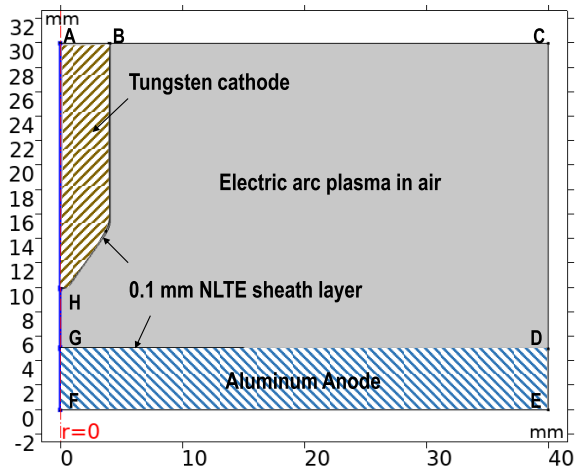

Fig. 2. Model setup for UPM-FEM in COMSOL.

The cathode/plasma and plasma/anode boundary layers (or sheath layers) are in the non-LTE discontinuity state [24]–[26]. In the modeling of the arc–material interactions, the electric current density, electric field, and magnetic field are solved by the current conservation equation and Maxwell's equations. The plasma fluid, modeled as a laminar flow, satisfies the conservation equations of mass and momentum. In the arc plasma domain, the volumetric heat source mainly includes thermal conduction, energy transfer from electronic enthalpy transport, Joule heating (coupled with the electric current equation), and radiation emission. The governing equations for the UPM-FEM are solved using finite-element analysis with COMSOL Multiphysics. Note that the UPM-FEM has already been validated in authors' prior work by the experimental results for an air electric arc problem with metal material anodes (e.g., stainless steel and aluminum) and also verified by a free-burning argon arc benchmark problem with copper anode [27]. Therefore, such work will not be repeated here. Below describes the numerical implementation of this model to allow readers to easily reproduce our results.

1) *Computational Domain:* Cathode–arc–anode domain (40 mm in width and 30 mm in height) in the 2-D cylindrical coordinates with axisymmetry along the arc center and with a 5-mm arc gap (as shown in Fig. 2).
2) *Physics (or Modulus) Used in COMSOL:* i) Electric current; ii) magnetic field; iii) heat transfer; and iv) laminar flow.
3) *Multiphysics Coupling Interfaces:* i) Equilibrium discharge heat source (for coupling the plasma heat sources with the heat transfer equation); ii) static current density component (for coupling the electric current with the magnetic field); iii) flow coupling (for coupling the laminar flow with the heat transfer interfaces); and iv) temperature coupling (for coupling the heat transfer with all other interfaces by passing the instant temperature solution to other field equations).
4) *Input Current:* A constant and uniform current density, J_{in} (see Table I) converted from a constant current of 404 A and applied at boundary "AB" (see Fig. 2).

TABLE I
SUMMARY OF THE BOUNDARY CONDITIONS USED IN THE UPM-FEM

	AB	BC & CD	DE	EF	DG	BH	AF
T	300 K	300 K	300 K	300 K	Ra	Ra	$\frac{\partial T}{\partial r}=0$
u	-	Open BC	0	0	0	0	$\frac{\partial \mathbf{u}}{\partial r}=0$
J	$\mathbf{J}\cdot\mathbf{n}=-J_{in}$	$\mathbf{n}\cdot\mathbf{J}=0$	-	-	-	-	$\frac{\partial \mathbf{J}}{\partial r}=0$
V	-	-	0	0	-	-	$\frac{\partial V}{\partial r}=0$
A	$\mathbf{n}\cdot\mathbf{A}=0$	$\mathbf{n}\cdot\mathbf{A}=0$	$\mathbf{n}\cdot\mathbf{A}=0$	$\mathbf{n}\cdot\mathbf{A}=0$	-	-	$\frac{\partial \mathbf{A}}{\partial r}=0$

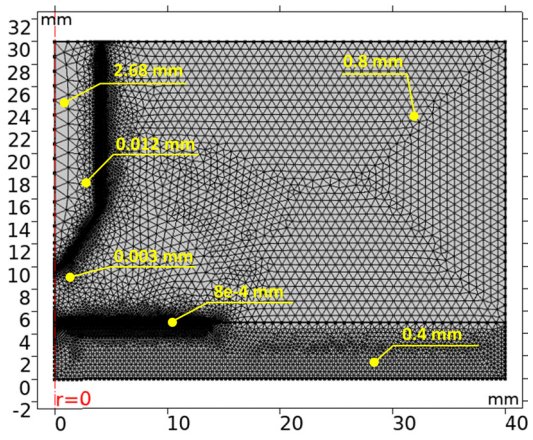

Fig. 3. Nonuniform mesh configuration used for the UPM-FEM with different mesh sizes at different regions.

5) *Boundary Conditions:* As shown in Table I, where "Ra" denotes the surface radiation, T is the temperature, u is the velocity, J is the current density, V is the electric potential, and A is the magnetic potential.
6) *Mesh:* User-controlled mesh with 14 016 triangle elements and nonuniform mesh sizes (as shown in Fig. 3).
7) *Material Properties of the Air Plasma:* Taken from [26] for temperatures up to 24 000 K and from [28] for temperatures beyond 24 000 K.
8) *Material Properties of the Anode (Aluminum) and Cathode (Tungsten):* Taken from the COMSOL material library. Note: the evaporation process and latent heating absorption of metal are considered.
9) *Damaged Depth Criteria:* The greatest penetration depth of the melting temperature in the material.
10) *Solver Settings and Computing Time:* Time-dependent solver, initial time increment of $1e^{-13}$ s, average computing time on a 16-GB Ram laptop of 30 min.

The long continuing lightning current, known as Component C in the lightning strike testing standard [20], has the largest charge transfer among the four typical lightning components and inflicts severest damage to the electrically conductive materials [9], [27]. A typical Component C current has a constant current of ~400 A and a duration of ~500 ms to fulfill the charge transfer of 200 C, as shown in Fig. 4.

The UPM-FEM can predict the distributions of temperature, velocity, pressure, and magnetic flux density in the

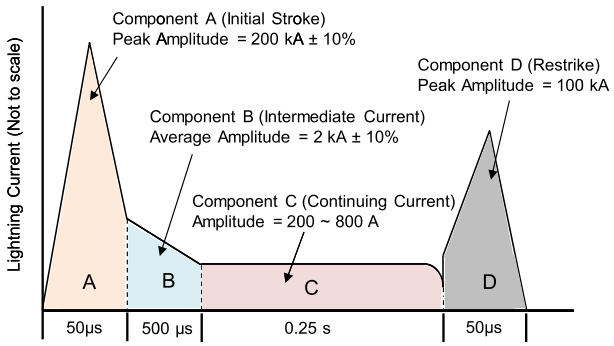

Fig. 4. Set of $A/B/C/D$ waveforms in the SAE standard [20].

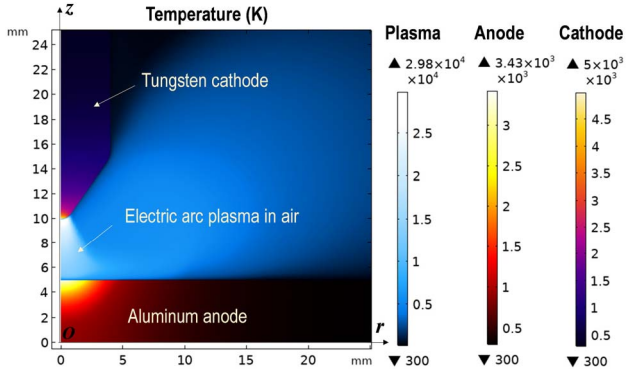

Fig. 5. Temperature distributions predicted by the UPM-FEM in the cathode–arc–anode domains in a typical lightning strike Component C current (constant current of 404 A and duration of 0.52 s).

cathode–plasma–anode domains, noting that these parameters still cannot be measured accurately in laboratory due to the extremely intense light emission and large current flow in the short-gap discharges. The temperature distributions predicted by the UPM-FEM in the cathode–arc–anode domain at the end of the analysis subjected to an arc discharge in air with the long continuing lightning current are demonstrated in Fig. 5.

III. INFLUENCE OF METAL VAPOR ON ARC PROPERTIES

The lightning arc is simulated using the proposed UPM-FEM with a constant current of 404 A and a duration of 520 ms. The target material is an Al alloy 3003. In our model, the metal is assumed to be damaged when the temperature exceeds its melting point (i.e., 933 K for Al 3003).

In response to the added metal vapor, the net emission coefficient will increase due to the stronger radiation phenomenon of plasma-arc-containing metallic elements [29]. The combined considerations of molecular bands, radiative recombination and attachment, and bremsstrahlung are essential to make predictions of the changes in the net emission coefficient. In the temperature range of 5000–25 000 K, the net emission coefficient can be altered as much as hundreds of times due to different concentrations of added metal vapor [25], [29]. As shown in Figs. 6 and 7, our simulations find that an increased net emission coefficient can significantly decrease the peak heat flux (from 19×10^7 to 6×10^7 W/m^2) and peak current density (from 2.7×10^7 to 0.6×10^7 A/m^2) at the arc attachment in consideration of such changes brought by the

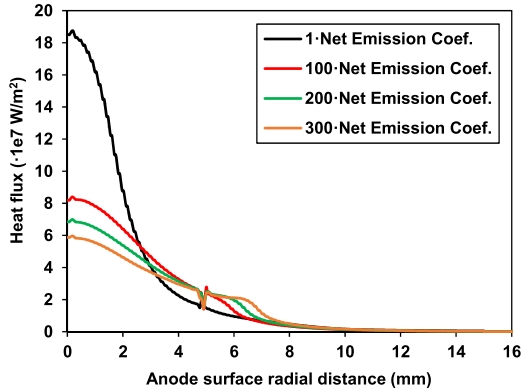

Fig. 6. Effect of increasing the net emission coefficient of the arc plasma on the heat flux flowing from the arc to the aircraft material (electric current 404 A, duration 520 ms, aluminum anode. "#·Net Emission Coef." represents the case in which we scaled up the net emission coefficient by # times).

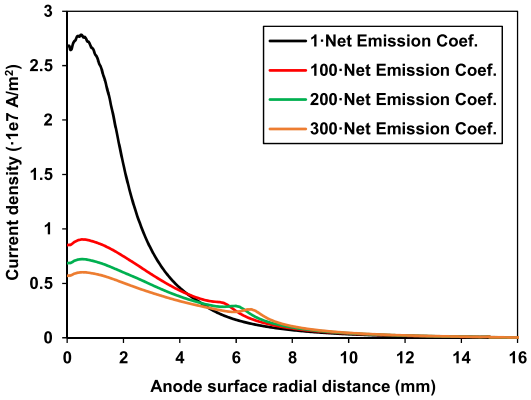

Fig. 7. Effect of increasing the net emission coefficient of the arc plasma on the current density flowing from the arc to the aircraft material (electric current 404 A, duration 520 ms, aluminum anode).

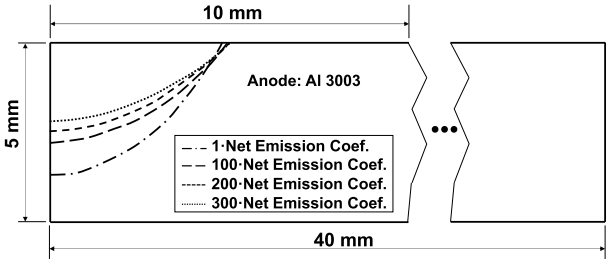

Fig. 8. Effect of increasing the net emission coefficient of the arc plasma on the damage of the aircraft metallic material (electric current 404 A, duration 520 ms, aluminum anode).

added metal vapor. Whereas it brings a moderate enhancement in both heat flux and current density at a radial distance of 3–8 mm from the central point of arc on the metal surface. Metal vapor results in a dramatic enhancement in the radiant power density, leading to a temperature decrease in the arc center. The variations in the net emission coefficient also lead to an obvious decrease in the damage depth (from 3.75 to 2.2 mm), but a slight increase (<1%) in the damage area, as shown in Fig. 8.

The electrical conductivity of arc is affected significantly by the presence of metal vapor in the temperature range

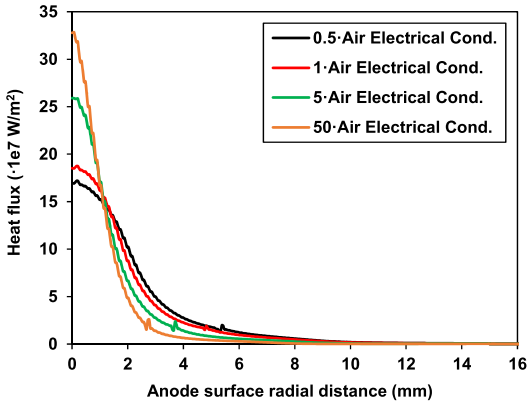

Fig. 9. Effect of increasing the electrical conductivity of the arc plasma on the heat flux flowing from the arc to the aircraft material (electric current 404 A, duration 520 ms, aluminum anode).

TABLE II
HEAT FLUX INTEGRAL OVER RADIAL DISTANCE ALONG THE METAL SURFACE

Integral of heat flux over radial distance (W/m)				
Net emission coefficient/ε_N	ε_N	$100\times\varepsilon_N$	$200\times\varepsilon_N$	$300\times\varepsilon_N$
	4.5×10^8	3.2×10^8	2.9×10^8	2.7×10^8
Electrical conductivity/σ	$0.5\times\sigma$	σ	$5\times\sigma$	$50\times\sigma$
	4.7×10^8	4.5×10^8	4.4×10^8	4.1×10^8
Thermal conductivity/k	$0.1\times k$	$0.5\times k$	k	$5\times k$
	2.3×10^8	3.7×10^8	4.5×10^8	5.4×10^8

of 5000–25 000 K with a reverse point of around 15 000 K. In particular, the electrical conductivity will increase by ~10 times or even more below this critical temperature (i.e., reverse point) and then decrease by ~20% or more at higher temperatures with added metal vapor [25]. Our simulation results show that the increase in the electrical conductivity will result in a growth (by ~200%) in the peak heat flux at arc attachment, as shown in Fig. 9. Despite the increase in the peak heat flux, the total heat flux decreases by ~14.6% based on the integral calculation along the metal surface (see Table II). This decrease in the total heat flux could be understood with the lower value of the heat flux (decreased by ~50%) at a radial distance of 2–8 mm along the metal surface, as shown in Fig. 9. The decrease in the total heat flux is considered one of the main reasons for causing reductions in the damage depth and damage area.

Moreover, the regions affected by a considerably higher heat flux become smaller (due to the pinch effects and arc radius contraction at higher current) and this will decrease the damage area. The current density shows a monotonic increase with electrical conductivity, as shown in Fig. 10. The higher current density generates stronger arc energy in the core arc region (radial distance <2 mm), leading to a further increase in the damage volume. As shown in Fig. 11, the damage area and damage depth of the metal are modified under different levels of electrical conductivity, of which the damage depth can decrease by 52% and the damage area contracts by 50% due to the enhancement of the electrical conductivity. But

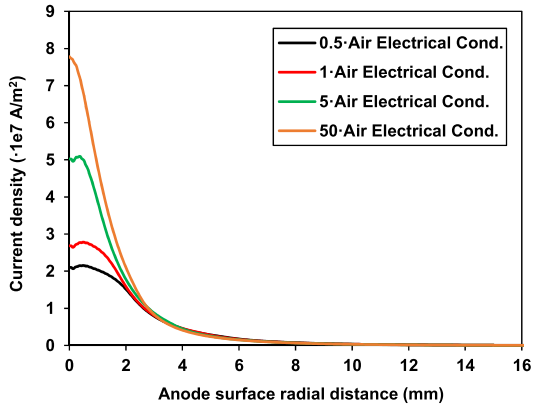

Fig. 10. Effect of increasing the electrical conductivity of the arc plasma on the heat flux flowing from the arc to the aircraft material (electric current 404 A, duration 520 ms, aluminum anode).

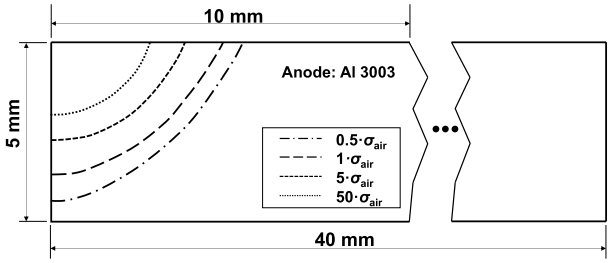

Fig. 11. Effect of increasing the electrical conductivity of the arc plasma on the damage of the aircraft metallic material (electric current 404 A, duration 520 ms, aluminum anode).

bearing in mind that if the arc temperature exceeds the reverse temperature point, the electrical conductivity will drop, which will lead to the rebound of the damage depth and area.

Metal vapor can alter the thermal conductivity and further affect the predictions of heat flux and current density, for example, an addition of 10 mol% metal vapor can double the thermal conductivity of the arc plasma for temperatures between 5000 and 12 000 K but will decrease the thermal conductivity by ∼50% when temperatures are higher than 12 000 K [25]. As shown in Figs. 12 and 13, our simulation results show that a decrease in the thermal conductivity (from k_{air} to $0.1 \times k_{\text{air}}$, k_{air} = thermal conductivity of air) can substantially lower down the peak heat flux (by ∼4 times) and also reduce the peak current density by ∼3 times for the regions within a radial distance of <2 mm on the anode surface. This leads to a contraction of the cross-sectional area of the arc channel. From k_{air} to $5 \times k_{\text{air}}$, the peak heat flux changes insignificantly but the integral of the total heat flux along the arc cross section has a noticeable increase of 20% (see Table II), the details of which will be discussed in the following context.

On the other hand, both the arc heat flux and current density profiles drop much faster along with the radial distance of the metal surface when the thermal conductivity is increased. The resultant damage area is expected to be mitigated due to this radial attenuation. Specifically, the damage depth is more sensitive to the increase in the thermal conductivity when compared with the damage area. This can be verified in Fig. 14 considering the arc–metal interactions and the metal

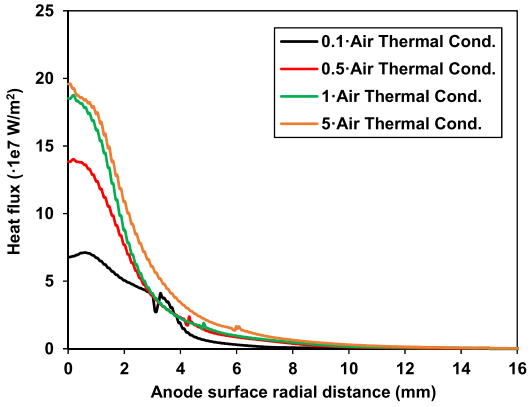

Fig. 12. Effect of changing the thermal conductivity of the arc plasma on the heat flux flowing from the arc to the aircraft material (electric current 404 A, duration 520 ms, aluminum anode).

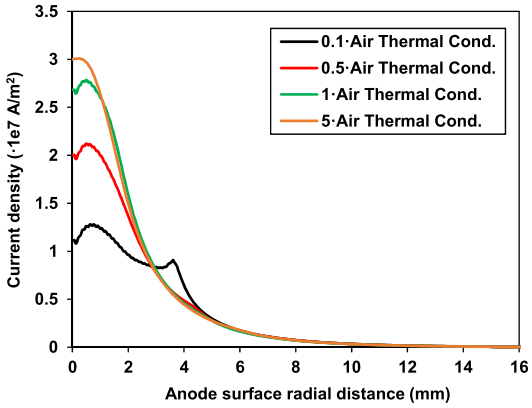

Fig. 13. Effect of changing the thermal conductivity of the arc plasma on the current density flowing from the arc to the aircraft material (electric current 404 A, duration 520 ms, aluminum anode).

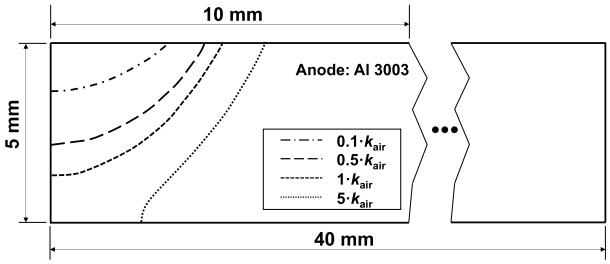

Fig. 14. Effect of changing the thermal conductivity of the arc plasma on the damage of the aircraft metallic material (electric current 404 A, duration 520 ms, aluminum anode).

melting process. The associated alterations in the heat flux and current density significantly change the damage depth (from 1.6 to >5 mm and even leading to a burn-through in the case of the fivefold increase in the thermal conductivity) and bring a relatively smaller change in the damage area (from a radius of 3 to >6.2 mm). The less significant change in the damage area could also be attributed to the intensified arc constriction due to the increase in the thermal conductivity of the plasma.

For conductive materials, the Joule heating can be neglected in the analysis of the direct lightning damage effects [9]. The arc energy is the main thermal source and can be roughly

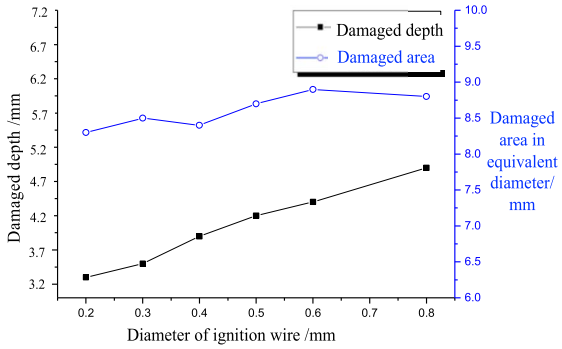

Fig. 15. Results of Al alloy struck by lightning in experiments with different diameters of ignition wires.

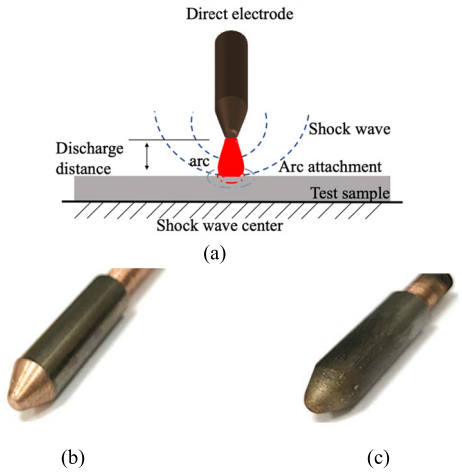

Fig. 16. (a) Direct electrode in a semiellipsoidal shape. Electrode (b) before and (c) after the simulated arc experiment.

indexed by the heat flux integral over the radial distance along the plasma-affected metal surface (note: the heat flux profile is roughly in the steady state in the case of a constant current). The results of the total heat flux integral to the changes in the net emission coefficient and the electrical and thermal conductivities are shown in Table II. The contamination by metal vapor can potentially lower down the integral of the heat flux by ∼2 times in a pathway of altering the net emission coefficient. The remarkable decrease in the heat flux integral leads to a moderate damage depth as shown in Fig. 8. Furthermore, due to the Gaussian-shape decrease profile of the heat flux along the material surface (see Fig. 6), the damage area did not experience a significant increase. The alterations in electrical conductivity bring a 14% decrease in the heat flux integral and have led to reduced damage depth as illustrated in Fig. 11. The integral of the heat flux can change more than 2 times in response to the alterations of thermal conductivity. If less heat flux is imposed on the metal surface, both the damage depth and area will be reduced (see Fig. 11). Therefore, the undesirable metal vapor produced from the ignition wire noticeably affects the damage depth through the main mechanism of alterations in the net emission coefficient and thermal conductivity and shows less influence on the damage area due to the Gaussian-shape decrease profile of the heat flux and its insensitivity to the changes in the net emission coefficient.

IV. Discussion

The electrode jet phenomenon is the movement of ions and vaporized particles originated from the electrode in arc discharge. The indirect electrode creates an obstruction on head to block the plasma jet impinging the tested material directly. Such a configuration greatly reduces the air breakdown ability of the cathode/anode, which necessitates the use of a metallic ignition wire between electrodes to create a conductive path first and then initiate the arc discharge. But the diameter of the ignition wire may change from one experiment to another, making the testing results dependent on the experimental setup. The uncertainty can reach 46.9% in the damaged depth and 9.4% in the damaged area, as shown in our experimental test results in Fig. 15. This clearly brings misinterpretation in lightning tests and leaves the cross-comparison obscure between different research works.

Meanwhile, the ignition wire absorbs energy through melting or evaporating itself, and thus decreases the total energy budget from the arc to the material. Concurrently, the consumed ignition wire generates a considerable volume of metal vapor and contaminates the arc column, which will change the transport properties and net emission coefficients (as discussed in Section III), leading to changes in the heat flux and current density. Besides, the dielectric cap itself would absorb partial arc energy and suppress the force impacts. The electric field strength in the vicinity of the electrode tip is significantly decreased and the ablation volume in the testing sample is reduced. In addition, the damage to materials is caused by a combination of the hot plasma heating and the shear forces through the expansion of over-pressure waves. In the indirect electrode configuration, it blocks the over-pressure waves [Fig. 1(a)] and restricts the expansion forces on the vulnerable quasi-liquid material (already melted by plasma heating), leading to questionable damage results.

Another alternative method for decreasing the influence of the electrode jet is to use a direct electrode and minimize the volume of vaporization in the electrode material. In addition, the discharge electrodes with different shapes will have distinct electric field profile on head. The electric field strength affects the subsequent dynamic electron density and the associated arc radius. Our previous study shows that the electrode in a semi-ellipsoidal shape [see Fig. 16(a)] can smooth the variation in the surface electric field and thereby alleviate material erosion on the electrode surface [15]. In the experiment, when testing with higher lightning arc currents (≥200 A), the extremely high-temperature rise on the anode can still exceed the melting point near the head region. But the electrode surface erosion becomes relatively moderate and is acceptable in the lightning tests (see an example shown in Fig. 16). It should be noted that the adjustment of the physical properties of the electrode material to reduce the surface erosion still remains a challenge at present.

In summary, for the use of indirect electrodes in lightning certification tests, the unavoidable metal vapor produced from the vaporization of the ignition wire significantly changes the arc energy density and heat flux. The influence on the arc

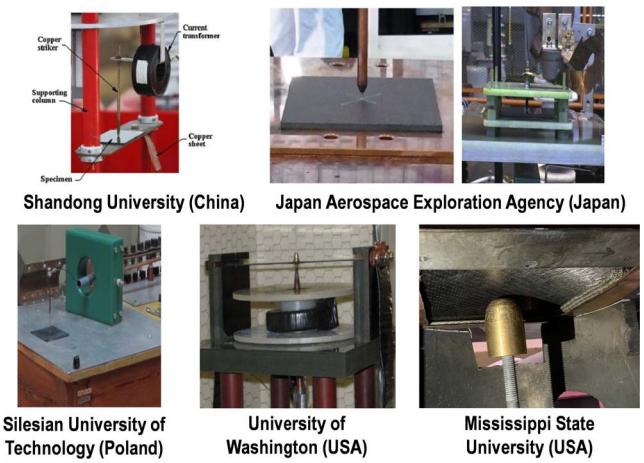

Fig. 17. Use of the direct electrode configuration in the existing lightning strike testing [30]–[36].

properties is uncontrollable due to the different content of the metal vapor contamination among experiments. In contrast, using the direct electrode can produce the unrestricted arc energy and resultant force impacts in lightning certification tests, achieving the consistency in lightning testing setup cross different experiments. It is also noted that the use of the direct electrode configuration has recently gained a momentum, as evidenced by many articles related to lightning strike testing published by researchers all over the world (see Fig. 17) [30]–[36], rendering a promising future for more accurate lightning certification tests.

V. Conclusion

In simulated lightning direct damage testing, a requisite ignition wire used in the indirect electrode configuration will considerably change the arc properties (i.e., net emission coefficient and transport properties) due to the addition of metal vapor contamination. Through numerical modeling, we found that the metal vapor added to the arc plasma can alter the total heat flux integrated over the material surface by 166.7% through a change in the net emission coefficient, by 234.8% through changing the thermal conductivity, and by 14.6% through changing the electrical conductivity. The damage depth of the tested material experienced a significant change of 312.5% caused by alterations in the net emission coefficient and thermal conductivity of the arc plasma due to the added metal vapor. The damage area shows moderate changes owing to a Gaussian-shape decrease profile of the heat flux and its insensitive response to the net emission coefficient (changed by less than 1%).

The direct electrode configuration eliminates the need for the ignition wire and is therefore free from the metal vapor contamination effect. Such a configuration can be taken as a promising solution, which translates to a testing condition in laboratory more representative to actual lightning conditions, and thus significantly improves the lightning strike protection design and development.

Acknowledgment

Y. Liu thanks J. Montanyà from Polytechnic University of Catalonia, Dr. A. Guha from Tripura University, and Dr. E. Williams, Dr. C. Zhang from the Massachusetts Institute of Technology for their valuable and constructive suggestions during the improvement of this research work. This work would not have been achieved without the assistance on the implementation of the simulated lightning experiments in Shanghai Jiao Tong University.

References

[1] F. Rachidi *et al.*, "A review of current issues in lightning protection of new-generation wind-turbine blades," *IEEE Trans. Ind. Electron.*, vol. 55, no. 6, pp. 2489–2496, Jun. 2008.
[2] P. Feraboli and H. Kawakami, "Damage of carbon/epoxy composite plates subjected to mechanical impact and simulated lightning," *J. Aircr.*, vol. 47, no. 3, pp. 999–1012, May 2010.
[3] J. A. Plumer, N. O. Rasch, and M. S. Glynn, "Recent data from the airlines lightning strike reporting project," *J. Aircr.*, vol. 22, no. 5, pp. 429–433, May 1985.
[4] V. Mazur, B. D. Fisher, and J. C. Gerlach, "Lightning strikes to a NASA airplane penetrating thunderstorms at low altitudes," *J. Aircr.*, vol. 23, no. 6, pp. 499–505, Jun. 1986.
[5] V. Rakov and M. Uman, *Lightning: Physics and Effects*. Cambridge, U.K.: Cambridge Univ. Press, 2003.
[6] E. R. Williams, "Lightning and climate: A review," *Atmos. Res.*, vol. 76, nos. 1–4, pp. 272–287, Jul. 2005.
[7] F. Fisher and J. Plumer, "Lightning protection of aircraft," Nat. Aeronaut. Space Admin., Sci. Tech. Inf. Office, Pittsfield, MA, USA, Tech. Rep. NASA Reference Publication 1008, 1977.
[8] Y. Liu, Z. Fu, A. Jiang, Q. Liu, and B. Liu, "FDTD analysis of the effects of indirect lightning on large floating roof oil tanks," *Electr. Power Syst. Res.*, vol. 139, pp. 81–86, Oct. 2016.
[9] Y. Liu, Z. Fu, Q. Liu, B. Liu, and A. Guha, "Experimental and analytical investigation on metal damage suffered from simulated lightning currents," *Plasma Sci. Technol.*, vol. 19, no. 12, Dec. 2017, Art. no. 125301.
[10] P. Foster, G. Abdelal, and A. Murphy, "Modelling of mechanical failure due to constrained thermal expansion at the lightning arc attachment point in carbon fibre epoxy composite material," *Eng. Failure Anal.*, vol. 94, pp. 364–378, Dec. 2018.
[11] Y. Wang and O. I. Zhupanska, "Lightning strike thermal damage model for glass fiber reinforced polymer matrix composites and its application to wind turbine blades," *Compos. Struct.*, vol. 132, pp. 1182–1191, Nov. 2015.
[12] V. Kumar *et al.*, "Factors affecting direct lightning strike damage to fiber reinforced composites: A review," *Compos. B, Eng.*, vol. 183, Feb. 2020, Art. no. 107688.
[13] G. Abdelal and A. Murphy, "Nonlinear numerical modelling of lightning strike effect on composite panels with temperature dependent material properties," *Compos. Struct.*, vol. 109, pp. 268–278, Mar. 2014.
[14] F. Moupfouma, "Aircraft structure paint thickness and lightning swept stroke damages," *SAE Int. J. Aerosp.*, vol. 6, no. 2, pp. 392–398, Sep. 2013.
[15] Y. Wang, "Multiphysics analysis of lightning strike damage in laminated carbon/glass fiber reinforced polymer matrix composite materials: A review of problem formulation and computational modeling," *Compos. A, Appl. Sci. Manuf.*, vol. 101, pp. 543–553, Oct. 2017.
[16] Y. Wang, "Modeling of lightning-induced thermal ablation damage in anisotropic composite materials and its application to wind turbine blades," Ph.D. dissertation, Dept. Mech. Eng., Univ. Iowa, Iowa City, IA, USA, 2016.
[17] X. Gao, B. Liu, Y. Liu, H. Xia, and Z. Fu, "Analysis on the choosing of test electrode for lightning current metal ablation experiments," in *Proc. 33rd Int. Conf. Lightning Protection (ICLP)*, Estoril, Portugal, Sep. 2016, pp. 1–6.
[18] K. Yousefpour, W. Lin, Y. Wang, and C. Park, "Discharge and ground electrode design considerations for the lightning strike damage tolerance assessment of CFRP matrix composite laminates," *Compos. B, Eng.*, vol. 198, Oct. 2020, Art. no. 108226.
[19] T. Sonehara, H. Kusano, N. Tokuoka, and Y. Hirano, "Visualization of lightning impulse current discharge on CFRP laminate," in *Proc. Int. Conf. Lightning Protection (ICLP)*, Shanghai, China, Oct. 2014, pp. 835–839.
[20] *Aircraft Lightning Test Methods*, Standard SAE-ARP-5416, US, 2013.
[21] *Recommended Practice for Lightning Protection of Aboveground Storage Tanks for Flammable or Combustible Liquids*, Standard API-RP-545, US, 2009.
[22] *Lightning Qualification Test Techniques for Aerospace Vehicles and Hardware*, Standard MIL-STD-1757A, US, 1996.

[23] *Aircraft Lightning Environment and Related Test Waveforms Standard*, Standard EUROCAE ED-84, EU, 1997.
[24] M. Schnick, U. Füssel, M. Hertel, A. Spille-Kohoff, and A. B. Murphy, "Metal vapour causes a central minimum in arc temperature in gas–metal arc welding through increased radiative emission," *J. Phys. D: Appl. Phys.*, vol. 43, no. 2, Jan. 2010, Art. no. 022001.
[25] M. Tanaka *et al.*, "Time-dependent calculations of molten pool formation and thermal plasma with metal vapour in gas tungsten arc welding," *J. Phys. D: Appl. Phys.*, vol. 43, no. 43, Nov. 2010, Art. no. 434009.
[26] M. Boulos, P. Fauchais, and E. Pfender, *Thermal Plasmas: Fundamentals and Applications*. New York, NY, USA: Springer, 2013.
[27] Y. Liu and Y. Wang, "Modeling the lightning continuing current electric arc discharge and material thermal damage: Effects of combinations of amplitude and duration," *Int. J. Thermal Sci.*, vol. 162, Apr. 2021, Art. no. 106786.
[28] A. D'Angola, G. Colonna, C. Gorse, and M. Capitelli, "Thermodynamic and transport properties in equilibrium air plasmas in a wide pressure and temperature range," *Eur. Phys. J. D*, vol. 46, no. 1, pp. 129–150, Jan. 2008.
[29] F. Lago, J. J. Gonzalez, P. Freton, and A. Gleizes, "A numerical modelling of an electric arc and its interaction with the anode: Part I. The two-dimensional model," *J. Phys. D: Appl. Phys.*, vol. 37, no. 6, pp. 883–897, Mar. 2004.
[30] S. Lampkin, W. Lin, M. Rostaghi-Chalaki, K. Yousefpour, Y. Wang, and J. Kluss, "Epoxy resin with carbon nanotube additives for lightning strike damage mitigation of carbon fiber composite laminates," in *Proc. Amer. Soc. Compos.*, Atlanta, GA, USA, Sep. 2019, pp. 1–12, doi: 10.12783/asc34/31338.
[31] Y. Liu, A. Guha, J. Montanya, Y. Wang, and Z. Fu, "Effects of single impulse current and multiwaveform multipulse currents on aluminum alloy in lightning damage analysis," *IEEE Trans. Plasma Sci.*, vol. 48, no. 4, pp. 1146–1153, Apr. 2020.
[32] Y. Li, R. Li, L. Lu, and X. Huang, "Experimental study of damage characteristics of carbon woven fabric/epoxy laminates subjected to lightning strike," *Compos. A, Appl. Sci. Manuf.*, vol. 79, pp. 164–175, Dec. 2015.
[33] T. Ogasawara, Y. Hirano, and A. Yoshimura, "Coupled thermal–electrical analysis for carbon fiber/epoxy composites exposed to simulated lightning current," *Compos. A, Appl. Sci. Manuf.*, vol. 41, no. 8, pp. 973–981, Aug. 2010.
[34] P. Feraboli and M. Miller, "Damage resistance and tolerance of carbon/epoxy composite coupons subjected to simulated lightning strike," *Compos. A, Appl. Sci. Manuf.*, vol. 40, nos. 6–7, pp. 954–967, Jul. 2009.
[35] A. Katunin, K. Krukiewicz, R. Turczyn, P. Sul, A. Łasica, and M. Bilewicz, "Synthesis and characterization of the electrically conductive polymeric composite for lightning strike protection of aircraft structures," *Compos. Struct.*, vol. 159, pp. 773–783, Jan. 2017.
[36] W. Lin, B. Jony, K. Yousefpour, Y. Wang, C. Park, and S. Roy, "Effects of graphene nanoplatelets on the lightning strike damage response of carbon fiber epoxy composite laminates," in *Proc. Amer. Soc. Compos.*, Sep. 2020, pp. 1–15, doi: 10.12783/asc35/34878.

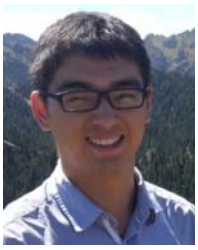

Yakun Liu (Member, IEEE) received the bachelor's degree in electrical engineering from Xi'an Jiao Tong University, Xi'an, China, in 2013, and the Ph.D. degree in electrical engineering from Shanghai Jiao Tong University, Shanghai, China, in 2018. He was also educated in civil and environmental engineering from the Massachusetts Institute of Technology, Cambridge, MA, USA.

His research interest focus on high-voltage technology, lightning protection, aerosol effects on lightning, and global lightning activity.

Yeqing Wang received the Ph.D. degree in mechanical engineering from University of Iowa, Iowa, IA, USA, in 2016.

He is currently an Assistant Professor with the Department of Mechanical and Aerospace Engineering, Syracuse University, Syracuse, NY, USA. His research interests include mechanics of composite materials and structures, lightning strike interaction with composite and metallic materials, composites in extreme environments (lightning strike, laser, plasma, and aerodynamic heating), and advanced multifunctional composite materials.

Dr. Wang was a Voted Member of the ASME Structures and Materials Technical Committee and a Senior Member of AIAA. He was a recipient of the Ralph E. Powe Junior Faculty Enhancement Award and the Best Paper Award at the 2012 American Society for Composites Technical Conference.